Graphite Structural Assessment through Acoustic Resonance and Machine Learning

Paul Geimer, Andrew Delorey, Rajarshi Bose, Anna Patelli

LA-UR-26-20537
January 30, 2026

Los Alamos
NATIONAL LABORATORY

Prepared for: U.S. Department of Energy
Office of Nuclear Energy
John H. Jackson, National Technical Director
DOE Microreactor Program

Prepared by: Paul Geimer, Scientist
Los Alamos National Laboratory

Acknowledgments

We are appreciative of past project contributions by Luke Beardslee and T.J. Ulrich, as well as the test sample which was acquired through the help of Erik Luther, Holly Trellue, and Tarik Saleh.

Summary

Nuclear microreactors offer the promise of flexible, deployable, and economically competitive clean-energy systems for remote installations, industrial applications, and microgrids. Their compact size and simplified designs, however, shift operational priorities toward extensive automation, reduced staffing, and long-duration operation with minimal maintenance. These requirements heighten the need for robust, in-situ structural health monitoring capable of detecting early signs of degradation in critical reactor components. Graphite, widely used for neutron moderation and structural support in reactor cores, presents unique monitoring challenges due to its quasi-brittle behavior, irradiation-induced dimensional change, and evolving internal stress fields. Conventional nondestructive evaluation techniques are difficult to deploy continuously inside small, high-temperature and -dosage reactor vessels, motivating development of alternative diagnostic approaches.

Building on recent efforts on vibration-based evaluation of graphite components, here we provide supplemental analyses of previously collected datasets and present additional findings on spatial defect localization from additional testing. This study explores a vibration-based nondestructive evaluation strategy that leverages broadband mechanical excitation, laser Doppler vibrometry, and a hybrid machine-learning (ML) framework built using graph neural networks and Fourier neural operators.

Building on prior demonstrations of accurate vibrational discrimination in nominally identical samples, we focus here on perturbations within a single, more complex component. Within a hexagonal graphite block, we introduced localized internal stresses via a reversible expanding-plug mechanism that were characterized at 75 - >90% accuracy using only external vibration measurements. These findings indicate that machine learning-enhanced analysis could provide a viable pathway toward non-intrusive, real-time monitoring in microreactor systems. Remaining challenges include deployment under irradiation, sensor integration in confined geometries, and ensuring model robustness under operational variability.

Contents

Figures

Contents

1 Introduction

Graphite has played a central role in nuclear energy since the earliest moderated reactors, where its low neutron absorption cross section and high thermal stability made it one of the first practical materials for neutron moderation and core structuring in fission systems [1]. Today, graphite remains integral to high-temperature gas-cooled reactors, many molten-salt concepts, and a growing number of proposed microreactor designs [2]. In these systems, graphite serves not only as a neutron moderator but also as a structural or flow-guiding component capable of retaining strength at elevated temperatures. For microreactors in particular—defined by compact geometries, extreme operating environments, minimal staffing, and expectations of long-duration autonomous operation—there is a growing need for approaches that can assess and track the mechanical condition of graphite components throughout their service life.

The appeal of graphite in reactor environments arises from its high-temperature stability, resistance to thermal shock, relatively low cost, and mature manufacturing base. At the same time, graphite is a highly complex engineering material. Its quasi-brittle behavior, hierarchical microstructure, and anisotropic crystallite orientation give rise to degradation mechanisms that evolve nonlinearly under irradiation and temperature. Neutron irradiation induces dose- and temperature-dependent changes such as dimensional change, irradiation creep, and degradation of elastic, thermal, and electrical properties, driven by defect accumulation, pore evolution, and crystallographic anisotropy [3]–[5]. The resulting mechanical response and fracture behavior are governed by a heterogeneous, multiscale microstructure comprising filler particles, binder phase, and interconnected porosity, with cracks initiating at pores or stress concentrators and propagating through microcrack coalescence across multiple length scales [1], [6], [7]. Recent experimental, microstructural, and modeling studies have significantly advanced understanding of graphite strength, damage tolerance, and lifetime prediction, supporting safety cases for current and next-generation graphite-moderated reactors [8]–[11]. Collectively, this highlights the challenge that even subtle changes in internal stress state or pore morphology could lead to measurable changes in material characteristics or dynamic behavior.

These sensitivities complicate inspection and condition assessment in operational reactor environments. Conventional nondestructive evaluation (NDE) techniques—including X-ray computed tomography, ultrasonic methods, eddy-current inspection, and neutron imaging—provide valuable insight into graphite structure and damage but are difficult to deploy in situ, particularly for microreactors. Small form factors, high temperatures, and intense radiation fields restrict access for sensors and human inspectors, while many NDE methods require line-of-sight, coupling media, or physical access that are incompatible with microreactor containment strategies. As a result, there is increasing interest in monitoring approaches that are minimally intrusive and amenable to continuous or periodic automated operation.

Structural health monitoring (SHM) based on vibration and modal analysis offers a promising alternative. Resonance frequencies, mode shapes, and broadband spectral features are inherently sensitive to changes in stiffness, density distribution, distributed microcracking, and boundary conditions. Such approaches have been applied in conventional reactor contexts to identify damage through shifts in dynamic signatures [12], [13]. Of particular relevance to compact microreactor designs, recent work has demonstrated the feasibility of optical-fiber-based vibration sensing in extreme environments [14], [15], including sustained operation at temperatures approaching 800°C [16]. A remaining challenge, however, lies in interpreting vibration data reliably and autonomously, with minimal reliance on human expertise.

Introduction

Machine learning (ML) provides a natural pathway toward addressing this challenge. Traditional reactor SHM is often performed manually or on fixed schedules, leaving substantial opportunity for data-driven methods to improve efficiency and sensitivity [17]. Modern ML techniques are well suited to extracting multidimensional patterns from broadband vibration data [18], and have been widely adopted in civil-structure SHM for their ability to learn meaningful features directly from continuous monitoring data without fully specified physics models [19]. A range of ML approaches has since been applied to SHM and NDE problems in metallic structures, e.g. [20], [21]. While graphite's comparably high porosity and internal damping can reduce signal sharpness, it has not precluded defect detection in surrogate graphite fuel elements [22].

Among numerous ML architectures in use, neural networks have proven broadly effective, with graph neural networks (GNNs) particularly well matched to spatially distributed sensing configurations. More recently, Fourier neural operators (FNOs) have emerged as a powerful framework for learning operator mappings in systems governed by partial differential equations [23], with applicability to wave propagation and elastic deformation phenomena. Their favorable generalization properties and computational efficiency have been demonstrated across a range of physical systems [23]–[25].

Motivated by these developments, this work discusses how distributed vibration measurements, interpreted through neural-operator-enhanced ML frameworks, performed to detect subtle structural changes in graphite components relevant to microreactor designs. Here, we demonstrate an approach combining laser Doppler vibrometry measurements with a hybrid FNO–GNN model to identify the status and location of internal changes within a hexagonal graphite block containing internal channels. The results illustrate how localized internal stress perturbations can produce learnable changes in vibrational response, with direct implications for the development of robust, minimally intrusive SHM strategies for future microreactor systems.

2 Materials and Methods

2.1 Sample Description

While work in the previous year included small populations of nominally identical graphite samples [26], we chose to focus defect localization efforts on a hexagonal monolith (graphite grade Mersen 2124) containing nineteen uniformly spaced axial channels. While not based on a specific reactor component design, the 10 x 30 cm hex block is intended to approximate the main geometric features of a reactor core block and is comparable to those used in recent test bed experiments [27]–[29]. The grade is isostatically molded for high strength and isotropic properties, characterized by fine grains (average sizes of 13 µm), high bulk density of 1.84 g/cm^3 (~80% theoretical density), open porosity of around 8%, and Young's moduli of approximately 11 GPa. These values align with those of graphite grades used in both historical and contemporary reactor designs [1], [30]. Although we note that small manufacturing and machining variations across a population can introduce spectral differences that are detectable through vibration-based analysis (e.g. Campbell et al. found a 4% variance in Young's moduli across 126 tested specimens of comparable Tokai grade G347 material [5]).

2.2 Experimental Setup

Here we describe the experimental approach for probing the steady-state vibration response under a range of stress conditions, including sample support, excitation, non-contact measurement, and the recoverable stress-perturbation used to test defect sensitivity. Data acquisition parameters, baseline material characterization, and the complementary FE modeling are also described.

Due to its relatively large mass and geometric complexity, the hexagonal block was supported by a sheet of open cell foam during testing, laying on one of its long faces. This arrangement minimized environmental vibrations and benchtop reflections and allowed the block to vibrate freely along the measurement surface with minimal additional damping. Such arrangements were important as graphite is relatively attenuating compared to steel used in previous tests with similar experimental protocols [31]. The quality factor of graphite (a measure of damping in an oscillator) can be an order of magnitude lower than steel, making resonance features less prominent in the vibration spectrum.

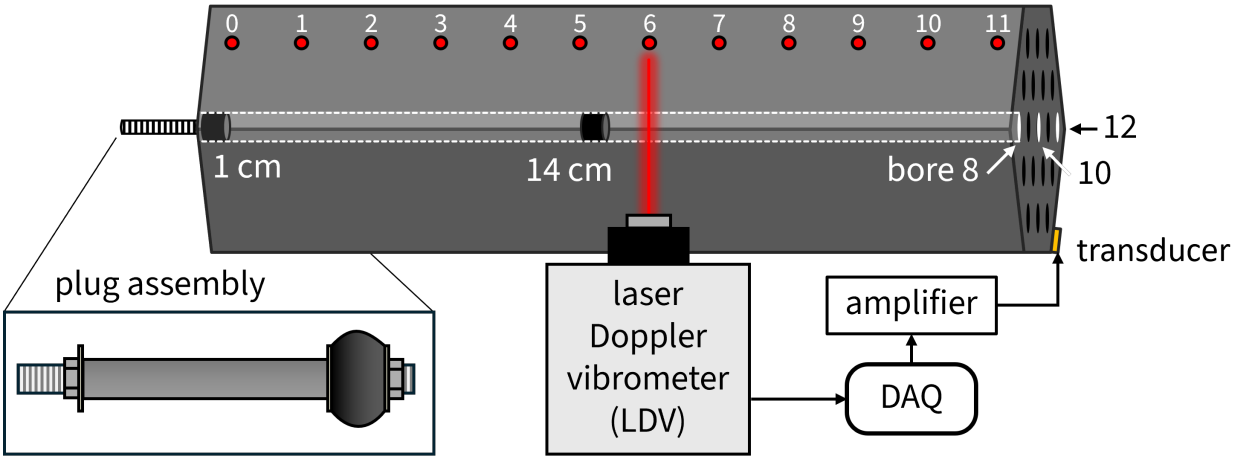

Figure 2-1: Experimental setup to test localization of internal stress applied via expanding rubber plug.

Materials and Methods

Mechanical excitation was produced by bare 2 mm × 12.7 mm lead-zirconate-titanate (PZT) disc transducer bonded to a small brass inertial backload. A drop of cyanoacrylate was used to adhere a transducer near one corner of the hex block to ensure repeatable contact as the sample was repositioned throughout the testing matrix. An arbitrary waveform generator (NI PXIe-5413) controlled by a LabVIEW interface supplied a repeatable white-noise input waveform, with signal voltage externally amplified by a factor of 20 (TEGAM model 2350) to produce sufficient vibration amplitudes across the audible and ultrasonic frequency ranges (Figure 2-1). White-noise excitation was chosen to approximate a passive monitoring scenario, where operational or ambient vibrations—rather than purpose-built shakers—would be utilized to provide broadband excitation.

Numerous approaches exist for measuring surface vibrations, including fiber-based sensors currently under development for reactor environments [16]. Though direct line-of-sight measurements are impractical in an operational setting, we employed a laser Doppler vibrometer (LDV) in this study to enable non-contact measurements with flexible placement. Vibration data were collected using a single-point LDV operating in the short-wavelength infrared (Polytec VibroFlex QTec), with the analog voltage output digitized via a scope card (NI PXIe-5122). The LDV operation included a translating configuration to acquire time-series data for ML training and testing. In this mode, the laser was fixed normal to the sample surface while the sample was translated in front of the beam, producing a discrete one-dimensional spatial dataset (Figure 2-2). The rotating configuration scanned discrete surface points with a moving laser spot, using galvanometer scanning mirrors (Thorlabs GVS012) were integrated inline with the LDV. Raster scanning under steady-state excitation at a series of resonance frequencies was used to obtain mode shapes and confirm modal behavior, following methods similar to those in [32], [33], with comparable alternatives reported elsewhere [34]. Together, these configurations ensured measurement consistency and enabled the collection of spatially distributed datasets for subsequent ML analysis.

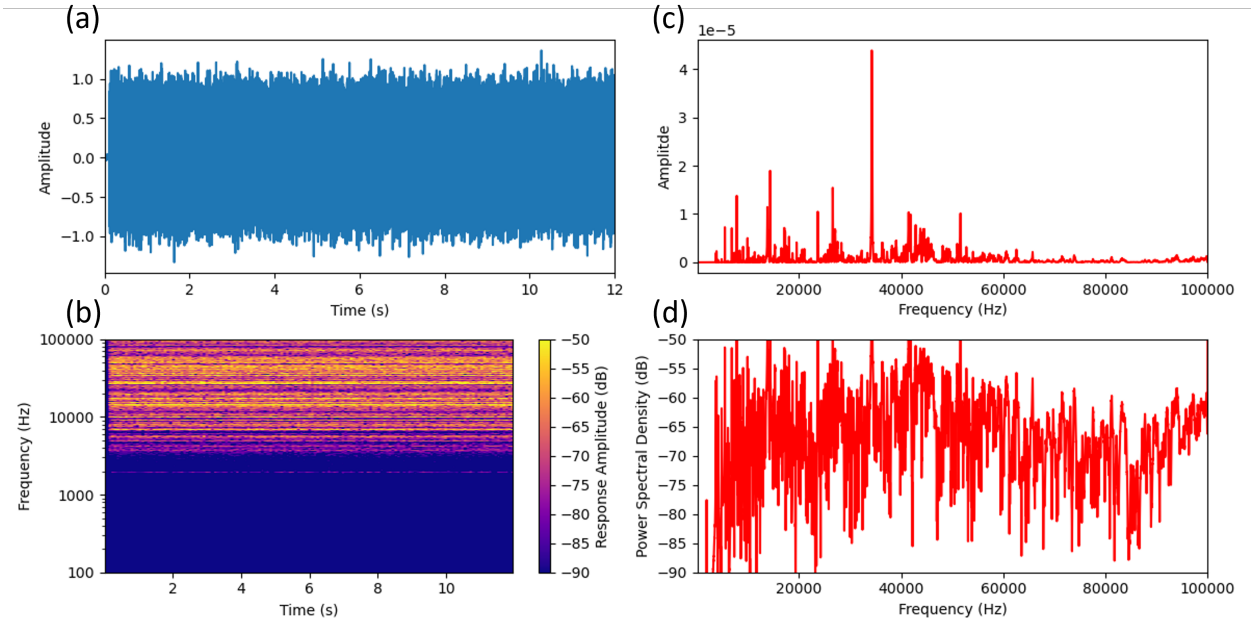

Figure 2-2: Typical vibration response data measured on the graphite hex block. (a) The raw time series at position 11 with the expanding plug inserted 14 cm within bore 10. Sample resonance is visible as horizontal lines in the spectrogram (b), or as peaks in the linear amplitude spectra (c) or power spectral density (d).

To evaluate the sensitivity of vibration-based methods to internal defects, a reversible, removable feature was desired to enable repeatable testing in multiple spatial dimensions. Localized heating was considered, but ultimately disregarded due to graphite's high thermal conductivity and the idle time needed for the system to return to thermal equilibrium. Due to past demonstration success when applying mechanical loading [31], [35], we chose to focus testing efforts on an artificial stress perturbation introduced inside the hexagonal block. A custom expanding-plug assembly—consisting of a rubber cylinder, metal washers, a threaded rod, and an outer compression nut—was inserted into selected axial channels (bores). Tightening the nut expanded the rubber element radially, imparting localized compressive and tensile stresses. This design enabled controlled and repeatable anomaly introduction without permanently damaging the sample. Multiple stress states were examined: a baseline without the plug inserted, as well as shallow and deep plug insertion depths into three different bores. These configurations were selected to evaluate binary anomaly detection as well as the model's ability to spatially discriminate between internal stress locations.

For each tested stress state, surface vibration measurements were collected at a sampling rate of 250 kHz along a linear array of 12 points spaced along the top surface, with their location motivated by prior modal imaging indicating large surface displacements in this region across multiple resonant frequencies (Figure 2-3). Each measurement consisted of a 60-s time series, yielding 15 million samples per location. In all time-series measurements, the LDV was configured with a bandwidth of 200 kHz and maximum range of 10 mm/s, which was the highest allowable sensitivity. These datasets provided the detailed spectral content for both modal analysis and ML feature extraction.

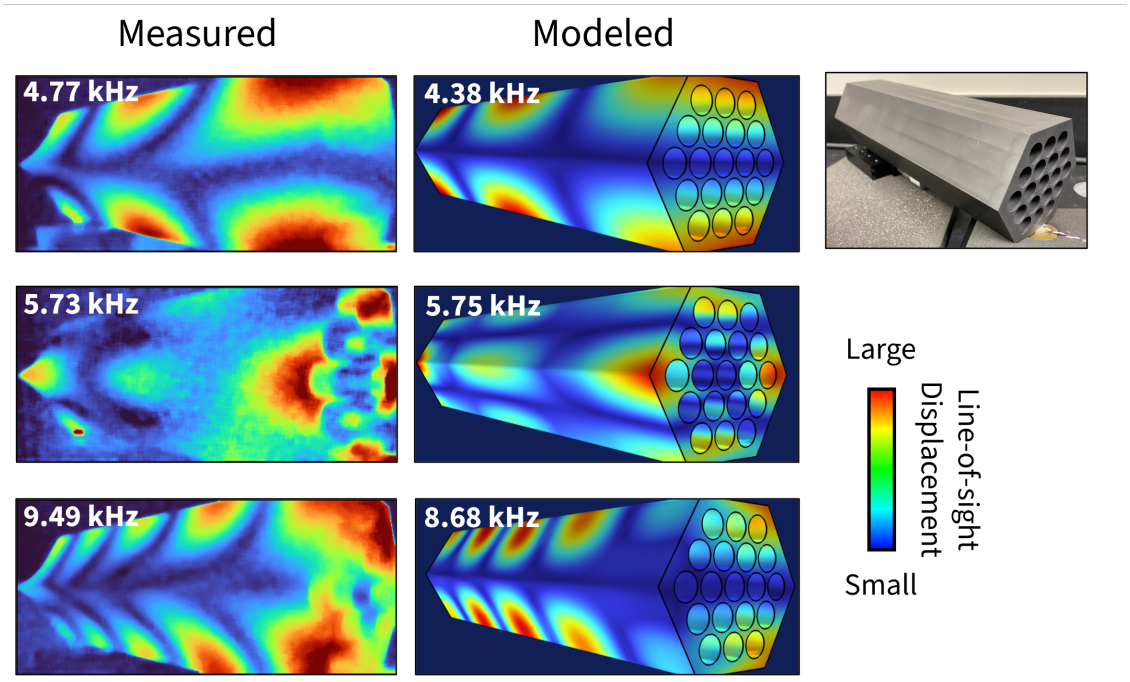

Figure 2-3: Examples of hex block mode shapes previously captured with scanning LDV (left) and matched against eigenmodes predicted by FEA for an isotropic model with free boundary conditions (right, modified from [26]. Warmer colors represent larger out-of-plane displacement. A cosine correction was applied to the FEA amplitudes to account for the changing angle of the laser during measurement. Photo shows setup used for both modal imaging and data acquisition for ML characterization.

Commercial finite-element analysis (FEA) software (COMSOL Multiphysics 6.3) was used to

calculate eigenvalues and eigenvectors of the hex block. These outputs were compared to the experimentally measured resonance frequencies and mode shapes to verify material properties, machining quality, and boundary-condition effects. FEA was also used to approximate the spatial distribution of the stresses induced by the inserted plug.

2.3 Machine Learning Framework

To efficiently extract defect-sensitive features from the vibrational response of graphite specimens for structural health monitoring (SHM), we employed a hybrid machine-learning framework that combines a graph neural network (GNN) with a Fourier neural operator (FNO). Although laser Doppler vibrometry (LDV) was used as the sensing modality in the present study, the model architecture is agnostic to the physical nature of the sensors, provided that all channels are recorded contemporaneously at a common sampling rate. This flexibility is motivated by anticipated deployment scenarios in microreactors, where surface-mounted and embedded sensors may be combined with passive vibration environments to enable continuous SHM [27]. By design, the framework supports heterogeneous and nonuniform sensing configurations without retraining or architectural modification.

The learning pipeline integrates spectral feature extraction with spatial reasoning across distributed measurements. Time-domain vibration signals are first transformed into a multi-spectral representation that emphasizes resonance behavior and broadband modal interactions relevant to vibration-based NDE. These features are then integrated across sensor locations to produce a component-scale representation, which is mapped to predicted elastic or structural states (e.g., plug presence, plug location, or sample identity). A more detailed description of the model architecture and training procedure is provided in Appendix A.

3 Results and Discussion

3.1 Localization of Internal Stress Anomalies

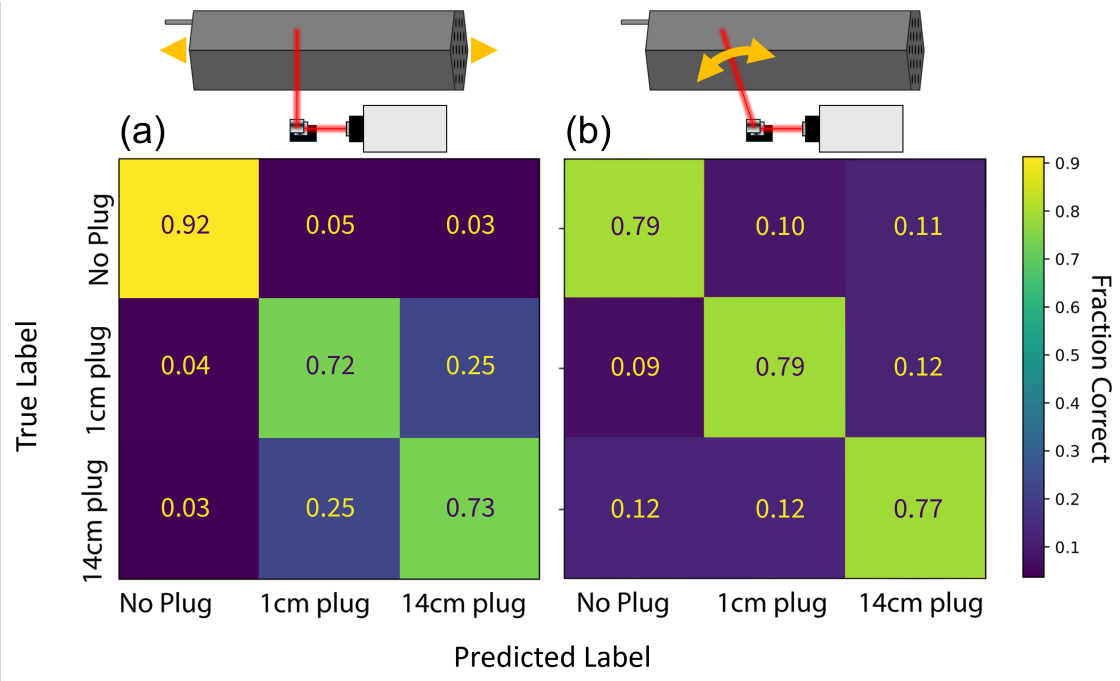

Figure 3-1: Comparison of 1D plug location predictions for two measurement schemes: (a) Stationary LDV beam while sample is translated across, previously reported in [26]. (b) Stationary sample while laser is relocated using scanning mirrors.

While one-dimensional plug localization was demonstrated in the prior year's work [26], we supplemented this result through a complementary test in which the same plug scenarios were tested, but using the rotating LDV configuration, where any repeatability issues related to repeatedly repositioning the sample in front of the beam were replaced by changing standoff distances and incidence angles as the mirrors redirected the laser across the sample. Our testing showed these two configurations to be largely comparable to one another (Figure 3-1). While the model was less successful at correctly distinguishing data collected with the plug absent, it demonstrated an improved capability to identify the one-dimensional location of the plug as either shallow (1 cm) or deep (14 cm) when installed. The relative parity of these two sets of predictions motivated the subsequent two-dimensional localization experiment to utilize the rotating LDV configuration in order to minimize sample and equipment movement.

In this separate test, the shallow and deep plug locations were maintained, while a second spatial dimension was added to the predictions by utilizing three of the longitudinal bores. 2D localization performance was observed to be largely comparable to the 1D test (Figure 3-2), with labels accurately predicted at rates of 84% - 96% across the five included plug scenarios (one of the shallow tests was discarded during final analysis due to previously unrecognized bias in the noise levels). Prediction accuracies were higher by about 5% for the shallow plug location. This indicates greater modal sensitivity in this region which is in agreement with the larger modal displacements that occur near the unconfined edges of a resonating geometry such as this hex block. Alongside

testing of spatial localization, we also used this dataset to evaluate the predictive performance gained by increasing the size of the graphs used in the ML model. Previous results here and in prior reports used simple one-node graph architectures, as this had been demonstrated to be sufficient to predict labels such as sample identity or sensor location with >99% accuracy. As the 2D spatial predictions left room for improvement in this case, we retrained on the same dataset using two-node graphs. This had the significant effect of improving prediction accuracy to rates of 97% - 99% across all five of the plug scenarios. Stated in the inverse, when averaged across the confusion matrix, the addition of a second graph point decreased the rate of incorrect predictions by about a factor of eight, from 12.2% to 1.6%. We also again note the marginally improved predictions when the plug was inserted at a shallow depth near the sample's outer face.

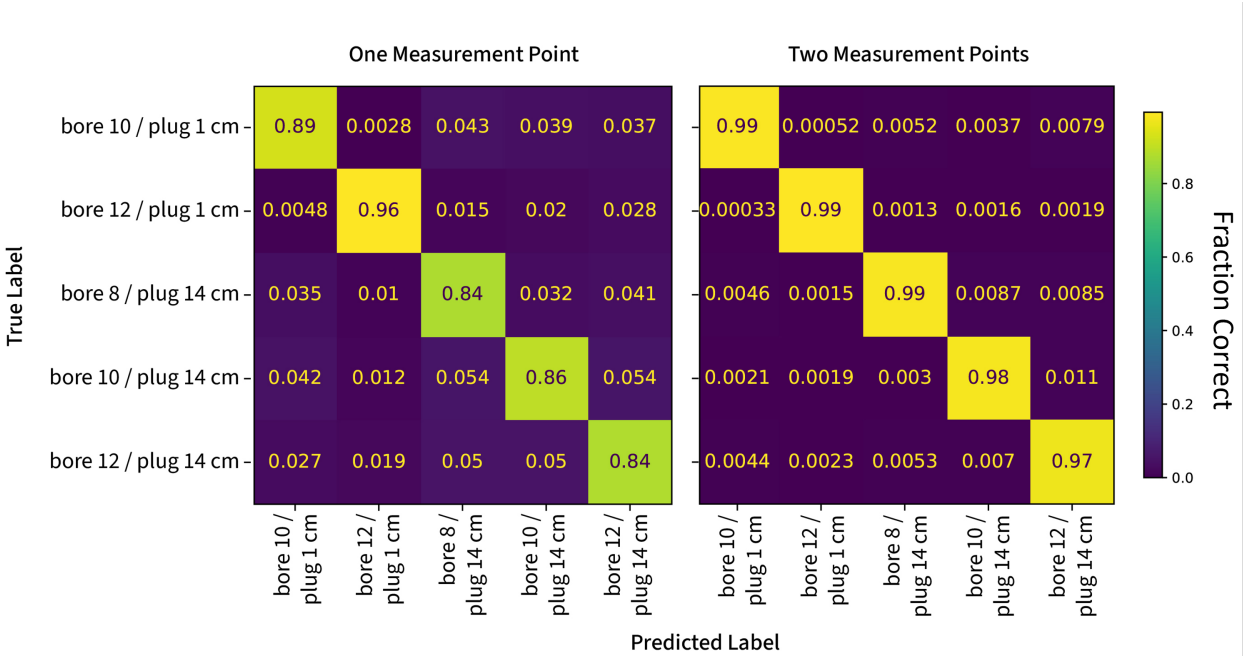

Figure 3-2: Confusion matrices for plug location predictions within hex block using FNO-GNN models employing one-node and two-node graphs.

3.2 Comparison to past results

While the level of prediction accuracy achieved in this study falls below the 99% accuracy generated from the same workflow when it was applied to artificial stresses within a stainless-steel hex block [26], a key difference is the relative volume of the sample that was stressed during each of the experiments. The stainless-steel sample was nearly uniformly compressed end-to-end, inducing stress across its entire length that corresponded to clear spectral shifts of several percent or more, as compared to the small internal volume affected by a compliant plug where a simple FEA study shows only 4% of the sample volume experienced more than 1% of the maximum applied stress (Figure 3-3). We note that the unique geometry of this block also served to generate a spatially varying combination of tensile and compressive stresses. While there are indications that unintended factors may have partially contributed to model accuracy in this study (see 3.3), the discrete spectral features learned within the model are sensitive to subtle, spatially distributed changes in wave

propagation and mode coupling induced by the internally complex stress fields. This is especially true in a ceramic material like graphite which has asymmetrically low tensile (vs. compressive) strength compared with many metals.

As shown in Figures 2-2 and 2-3, the graphite hex block exhibited rich modal behavior within the audible frequency range and above. These comparisons confirmed that the modal response of the block was governed primarily by its intrinsic geometry and material properties rather than boundary conditions, enabling meaningful assessment of perturbations generated within its internal channels. From an SHM perspective, these results indicate that ML-enhanced vibration analysis may be sensitive to the type of perturbations directly relevant for reactor-grade graphite components, which are likely to go through early-stage irradiation-induced swelling followed by shrinkage, along with the potential for contact stresses associated with other materials present in the core. This is supported by Pyun et al.'s recent SHM-with-ML study on graphite pebble quality assurance for other reactor designs [22].

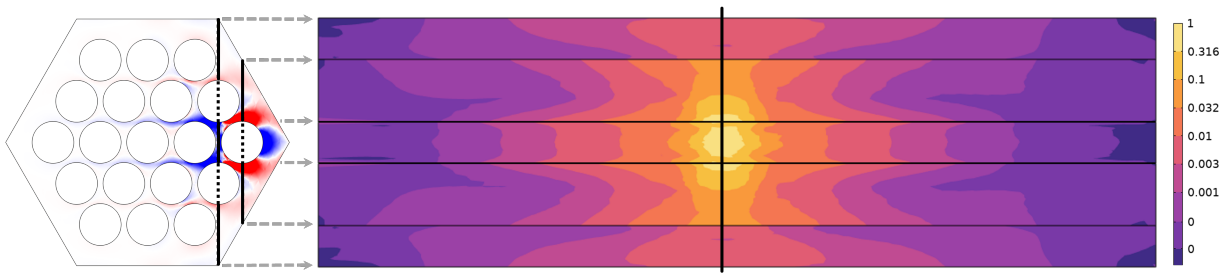

Figure 3-3: 2D cross sections of normalized stress for the deep plug configuration. (left) The σ_{xx} stress component (aligned left-right), with tension shown in red and compression in blue. (right) von Mises stress shown at two longitudinal slices through the block near the plug location. Color scale is logarithmic and discretized into half-decade bands.

3.3 Noise fluctuations

While the results reported herein demonstrate that a localized compressive stress within a single axial channel can meaningfully alter surface vibration signatures, it is important to consider whether variations in measurement noise may have influenced model predictions. In data-driven structural health monitoring, unintended correlations between noise characteristics and class labels can lead to artificially inflated performance if not properly examined.

To investigate this possibility, we examined model behavior and spectral characteristics using several complementary analyses. First, we revisited loss-function behavior observed during sample-identification tasks from prior work involving eight graphite spheres [26]. In that dataset, the fundamental resonance occurred near 21 kHz. When the maximum frequency content of the training data was incrementally increased from 1 kHz to 50 kHz, the loss function had already decreased by approximately 80% before reaching the fundamental resonance frequency. This observation suggests that a substantial portion of the model's learning could arise from spectral features not directly associated with dominant bulk resonances. Such features may include subtle material inhomogeneities that influence wave propagation, but they could also reflect artificial differences in background noise levels between measurements.

To quantify noise variability in the present study, we computed the median spectral amplitude within non-resonant frequency bands for each of the 60 independent measurements (five plug configurations across twelve measurement locations), see representative spectra in Figure 3-4. This

analysis revealed notable variation in noise floor between measurement locations, with the highest average noise level approximately 2.8× greater than the lowest. In contrast, noise levels were considerably more consistent across plug configurations: four of the five plug states exhibited noise floors within 12% of one another. The remaining configuration (bore 8, plug depth 14 cm) showed a noise floor approximately 60% higher than the lowest case; however, this elevated noise level did not correspond to improved classification accuracy in either the one-node or two-node graph models.

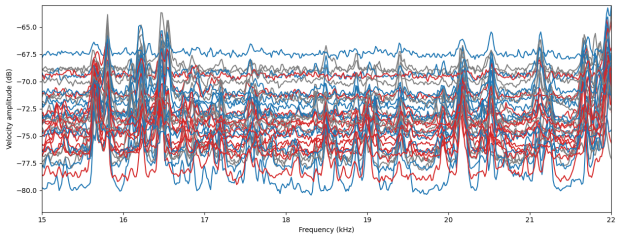

Figure 3-4: Comparison of noise across 12 measurement locations within spectral band containing a high density of resonance peaks. While the levels individual stations can be seen as outliers, the average noise for each plug configuration was found to be generally consistent. Curves from three configurations are shown for clarity (absent - blue, 1 cm - red, 14 cm - grey).

Taken together, these analyses suggest that while spatial variations in noise likely contribute to measurement-location-specific biases, they do not fully explain the observed classification and localization performance. The consistency of predictions across plug configurations suggests the model is responding to stress-induced changes in the vibrational response. Nonetheless, improved control of noise characteristics and additional validation under varying excitation and boundary conditions will be important for future studies aimed at deployment in operational reactor environments.

4 Conclusions and Future Work

In this study, we found ML-based acoustic NDE can localize a demonstration stressor in a geometrically complex graphite components relevant to microreactor applications. As compared to previous years' efforts, we found the FNO-GNN architecture generalized into multiple spatial dimensions and performed well amid spectral contamination and noisy source characteristics. Internal stress anomalies are especially relevant for microreactors, where graphite components in reactors may undergo irradiation-induced differential swelling and experience stress anomalies. In an operational setting, this approach would be also be suitable for ongoing monitoring whereby the model could be updated at regular intervals through inputs collected from an embedded sensor array, and validated with other independent measurements.

Detecting structural changes early is one key to maintaining reactor reliability, before they propagate into larger cracks or block-to-block contact forces that evolve beyond acceptable levels. The ability to detect stress anomalies using only external surface vibration measurements suggests that similar ML-driven workflows could be embedded in future microreactor designs using hardened sensors in similar locations, such as fiber-optic sensors bonded to inaccessible components of interest [16]. While there are other challenges to address outside those mentioned in this report (e.g. data storage, frequency content as related to localization accuracy), ML SHM systems likely have a role to play in microreactor designs and their planned semi-autonomous control [17].

This approach and/or comparable ML workflows could benefit from testing using a relevant sensor technology array on a test bed exposed to a stressor with more granular spatial positioning or cyclical loading. This will enable improved characterization of the technique's generalizability in changing conditions relevant to those within an operating reactor. This could generate a valuable test case to detect the onset of progressive damage, and evaluate the ability of a sparse array to localize such a feature in multiple spatial dimensions. There is also value in moving towards physics-informed ML approaches that may improve interpretation of model performance and sensitivity. Together, these advances can help establish vibration-based ML models as practical SHM tools for small nuclear concepts.

A Details of ML implementation

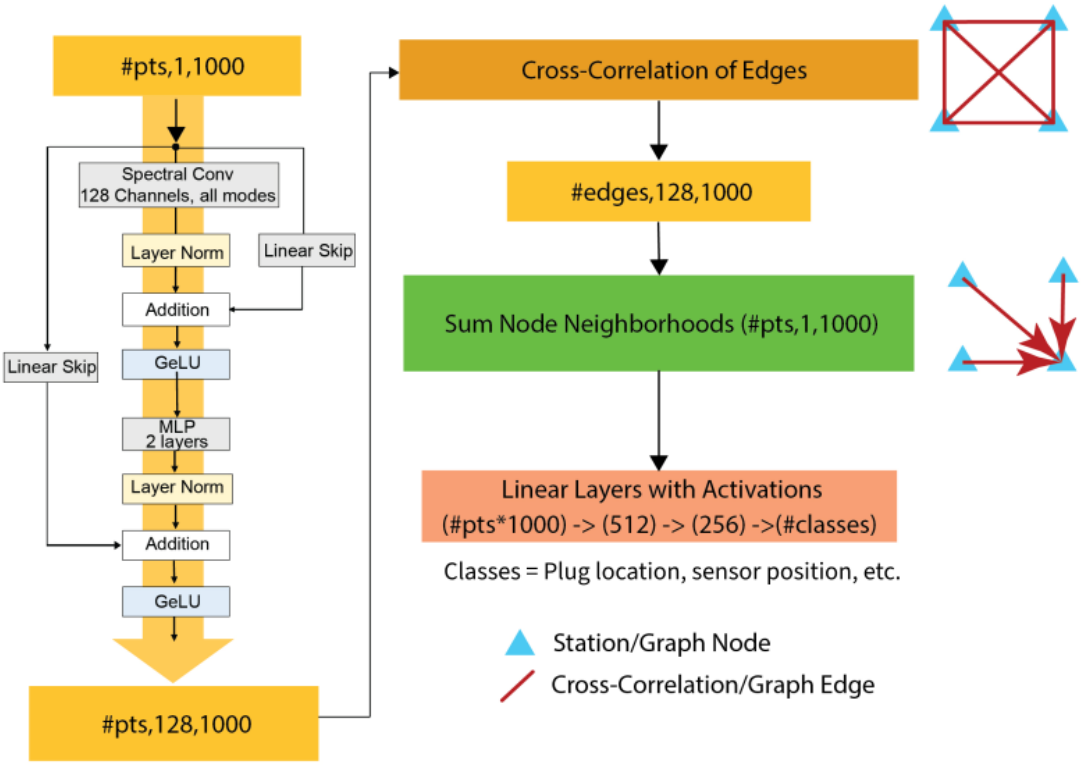

Figure A-1: Schematic diagram of FNO-GNN model architecture. FNO diagram (left) modified from [36]. GeLU - Gaussian error Linear Unit, activation function, MLP - multilayer perceptron.

The hybrid machine-learning architecture employed in this study couples a graph neural network (GNN) with a Fourier neural operator (FNO) to jointly capture spectral and spatial characteristics of measured vibrational responses. This approach is designed to integrate distributed sensing data across irregular geometries and sensor layouts, while remaining agnostic to sensor modality. Each measurement location—whether an LDV surface point in the present experiments or a potential embedded sensor in future deployments—is treated as a node in a graph. This formulation provides a flexible and physically intuitive representation of distributed sensing, particularly well suited to nonuniform sensor layouts and complex component geometries. While measurements in this study were acquired on a regular grid, the graph-based representation imposes no such requirement.

Each node contains a vibration time-series measurement, and edges encode relationships between pairs of nodes. The GNN is implemented as a message-passing graph using the PyTorch Geometric framework. Message passing at layer k is defined as:

$$x_i^{(k)} = \sum_N \varphi^{(k)}(x_i^{(k-1)}, x_j^{(k-1)}, e_{j,i}) \tag{1}$$

where x_i denotes the embedding of node i at layer k, $\phi^{()}$ is the learned message function, and $e_{j,i}$. Messages are aggregated at each node via summation.

Rather than operating directly on raw time-domain signals, each node's time series is first transformed using a Fourier neural operator. Neural operators generalize conventional neural networks by

Details of ML implementation

learning mappings between infinite-dimensional function spaces, typically implemented via integral operators [23]. In the FNO, these operators are realized in the Fourier domain, enabling efficient learning of global spectral correlations. By elevating each sensor channel into a higher-dimensional spectral representation, the FNO exposes resonance features, nonlinear interactions, and broadband spectral signatures that are critical for vibration-based nondestructive evaluation [24]. Unlike traditional modal analysis approaches that track a limited number of modal frequencies, the FNO learns directly from the full accessible spectrum. Our FNO implementation uses the Neural Operators Python package written in PyTorch by Jean Kossaifi, David Pitt, Nikola Kovachki, Zongyi Li, and Anima Anandkumar (https://neuraloperator.github.io).

The Fourier Neural Operator Block (FNOBlock) is embedded directly into the message-passing stage of the GNN. The input to the GNN is a tensor with dimensions (# of observation points, 1, 1000). Each observation is 1000 points from the vibration time series sampled at 250 kHz. Each observation point represents one node in the graph. Edges have the dimensions (#pts(#pts-1)/2, 1, 1000) as nodes are fully connected. In the message() function of the graph, each of the node time series is expanded with an FNOBlock:

```
FNOBlock(in_channels=1, outchannels=128, n_modes=501, channel_mlp_skip='linear',
fno_skip='linear)
```

After expansion, the edges have the dimensions (#pts(#pts-1)/2, 128, 1000). The cross-correlation outputs are processed through a sequence of one-dimensional convolutional layers with kernel size 3 and stride 1, arranged as: Conv1d, GELU, Conv1d, LayerNorm, Conv1d, GELU, Conv1d, Conv1d, LayerNorm. The final Conv1d layer reduces the channel dimension back to its pre-FNO size, yielding tensors of shape (N,1,1000). Following message passing and aggregation, node embeddings are pooled to form a component-scale representation. This representation is passed through a series of fully connected layers with nonlinear activation to produce predictions corresponding to the target classification task (e.g., plug presence, plug location, or sample identity).

Training data consisted of thousands of 4-ms time-series windows extracted from multi-second LDV recordings at each measurement location. Windows were randomly assigned to training, validation, and test sets to create statistical independence. Both single- and dual-node graphs were tested to assess how the model would generalize across different sensing densities.

All models were trained on a system equipped with an AMD EPYC Genoa 9334 CPU (32 cores, 64 threads), an NVIDIA L40S GPU, and 768 GB of RAM. In this configuration, a single training epoch required 10 minutes or less for the hex block dataset. Training proceeded until 50 consecutive epochs showed no improvement in validation performance, typically completing within several hours. Training and validation curves exhibited consistent convergence with no evidence of overfitting, indicating effective regularization arising from the combination of Fourier-domain feature extraction and graph-based message passing.

References

[1] J. D. Arregui-Mena, R. N. Worth, W. Bodel, *et al.*, "Multiscale characterization and comparison of historical and modern nuclear graphite grades," *Materials Characterization*, vol. 190, no. June, 2022, ISSN: 10445803. DOI: 10.1016/j.matchar.2022.112047.

[2] B. Zohuri and P. McDaniel, *Advanced Smaller Modular Reactors: An Innovative Approach to Nuclear Power*. Springer, 2019, pp. 1–220, ISBN: 9783030236823. DOI: 10.1007/978-3-030-23682-3.

[3] B. J. Marsden, M. Haverty, W. Bodel, *et al.*, "Dimensional change, irradiation creep and thermal/mechanical property changes in nuclear graphite," *International Materials Reviews*, vol. 61, no. 3, pp. 155–182, 2016, ISSN: 17432804. DOI: 10.1080/09506608.2015.1136460.

[4] T. Tanabe, "Radiation Damage of Graphite-Degradation of Material Parameters and Defect Structures," *Physica Scripta*, vol. 64, pp. 7–16, 1996.

[5] A. A. Campbell, Y. Katoh, M. A. Snead, and K. Takizawa, "Property changes of G347A graphite due to neutron irradiation," *Carbon*, vol. 109, pp. 860–873, 2016, ISSN: 00086223. DOI: 10.1016/j.carbon.2016.08.042.

[6] M. R. Joyce, T. J. Marrow, P. Mummery, and B. J. Marsden, "Observation of microstructure deformation and damage in nuclear graphite," *Engineering Fracture Mechanics*, vol. 75, no. 12, pp. 3633–3645, 2008, ISSN: 00137944. DOI: 10.1016/j.engfracmech.2007.11.003.

[7] D. Liu, K. Mingard, O. T. Lord, and P. Flewitt, "On the damage and fracture of nuclear graphite at multiple length-scales," *Journal of Nuclear Materials*, vol. 493, pp. 246–254, 2017, ISSN: 00223115. DOI: 10.1016/j.jnucmat.2017.06.021.

[8] R. Moskovic, P. J. Heard, P. E. Flewitt, and M. R. Wootton, "Overview of strength, crack propagation and fracture of nuclear reactor moderator graphite," *Nuclear Engineering and Design*, vol. 263, pp. 431–442, 2013, ISSN: 00295493. DOI: 10.1016/j.nucengdes.2013.05.011.

[9] B. Liu, H. Zhao, X. Li, Z. Yang, D. Zhang, and Z. Liu, "Effect of pore structure on the thermophysical and frictional properties of high-density graphite," *Microporous and Mesoporous Materials*, vol. 330, no. June 2021, p. 111 613, 2022, ISSN: 13871811. DOI: 10.1016/j.micromeso.2021.111613.

[10] M. Metcalfe, "Damage tolerance in the graphite cores of UK power reactors and implications for new build," *Nuclear Engineering and Design*, vol. 406, no. February, p. 112 237, 2023, ISSN: 00295493. DOI: 10.1016/j.nucengdes.2023.112237.

[11] W. Bodel, P. Martinuzzi, B. Davies, A. Steer, T. Lowe, and P. Mummery, "Mimicking irradiation-induced cracking of nuclear graphite using bromine intercalation," *Scripta Materialia*, vol. 199, pp. 10–13, 2021, ISSN: 13596462. DOI: 10.1016/j.scriptamat.2021.113889.

[12] O. Berg, J. Eiler, H. E. Garcia, *et al.*, *On-line Monitoring for Improving Performance of Nuclear Power Plants, Part 2: Process and Component Condition Monitoring and Diagnostics*. 2008. [Online]. Available: https://www-pub.iaea.org/MTCD/Publications/PDF/Pub1323%7B%5C_%7Dweb.pdf.

[13] IAEA, "Advanced surveillance, diagnostic and prognostic techniques in monitoring structures, systems and components in nuclear power plants," p. 139, 2013.

References

[14] A. Elshafey, H. Marzouk, X. Gu, M. Haddara, and R. Morsy, "Use of fiber Bragg grating array and random decrement for damage detection in steel beam," *Engineering Structures*, vol. 106, pp. 348–354, 2016, ISSN: 18737323. DOI: 10.1016/j.engstruct.2015.10.046.

[15] G. Laffont, R. Cotillard, N. Roussel, R. Desmarchelier, and S. Rougeault, "Temperature resistant fiber bragg gratings for on-line and structural health monitoring of the next-generation of nuclear reactors," *Sensors (Switzerland)*, vol. 18, no. 6, 2018, ISSN: 14248220. DOI: 10.3390/s18061791.

[16] A. Birri, D. C. Sweeney, H. C. Hyer, B. Schreiber, E. Cakmak, and C. M. Petrie, "A Miniaturized, High-Bandwidth Optical Fiber Fabry-Perot Cavity Vibration Sensor Demonstrated up to 800 °C," *IEEE Sensors*, vol. 25, no. 7, pp. 11 082–11 091, 2025, ISSN: 15581748. DOI: 10.1109/JSEN.2025.3541557.

[17] J. E. Daw, M. Good, R. Meyer, P. Ramuhalli, and L. Breon, "Assessment of Acoustic Sensor Application to Structural Health Monitoring of Reactor Components," Idaho National Laboratory (INL), Idaho Falls, ID (United States), Tech. Rep., 2022. DOI: 10.2172/2203075. [Online]. Available: https://www.osti.gov/biblio/2203075.

[18] C. R. Farrar, N. Dervilis, and K. Worden, "The Past, Present and Future of Structural Health Monitoring: An Overview of Three Ages," *Strain*, vol. 61, no. 1, 2025, ISSN: 14751305. DOI: 10.1111/str.12495.

[19] C. R. Farrar and K. Worden, *Structural health monitoring: a machine learning perspective*. John Wiley & Sons, 2012.

[20] J. Xiao and F. Cui, "Machine learning enhanced characterization of surface defects using ultrasonic Rayleigh waves," *NDT and E International*, vol. 140, no. October, p. 102 969, 2023, ISSN: 09638695. DOI: 10.1016/j.ndteint.2023.102969.

[21] G. Lv, S. Guo, D. Chen, *et al.*, "Laser ultrasonics and machine learning for automatic defect detection in metallic components," *NDT and E International*, vol. 133, no. August 2022, p. 102 752, 2023, ISSN: 09638695. DOI: 10.1016/j.ndteint.2022.102752.

[22] D.-K. Pyun, S. Lee, R. P. Palanisamy, *et al.*, "Comprehensive defect evaluation of advanced nuclear fuels using high-resolution acoustic signals and optimized sensor separation," *NDT & E International*, vol. 157, p. 103 502, Jan. 2026, ISSN: 09638695. DOI: 10.1016/j.ndteint.2025.103502.

[23] Z. Li, N. Kovachki, K. Azizzadenesheli, *et al.*, "Fourier Neural Operator for Parametric Partial Differential Equations," *ICLR 2021 - 9th International Conference on Learning Representations*, no. 2016, pp. 1–16, 2021. arXiv: 2010.08895.

[24] S. Qin, F. Lyu, W. Peng, *et al.*, "Toward a Better Understanding of Fourier Neural Operators from a Spectral Perspective," *CoRR*, 2024. arXiv: 2404.07200. [Online]. Available: http://arxiv.org/abs/2404.07200.

[25] C. Kaewnuratchadasorn, J. Wang, and C. W. Kim, "Neural operator for structural simulation and bridge health monitoring," *Computer-Aided Civil and Infrastructure Engineering*, vol. 39, no. 6, pp. 872–890, 2024, ISSN: 14678667. DOI: 10.1111/mice.13105.

[26] P. R. Geimer and A. A. Delorey, "Non-destructive structural characterization of graphite components using mechanical resonance and deep learning," Los Alamos National Laboratory, Tech. Rep., 2025, LA–UR–25–29 538.

[27] P. Sabharwall, J. L. Hartvigsen, T. J. Morton, *et al.*, "Nonnuclear Experimental Capabilities to Support Design, Development, and Demonstration of Microreactors," *Nuclear Technology*, vol. 209, no. sup1, S41–S59, 2023, ISSN: 19437471. DOI: 10.1080/00295450.2022.2043087. [Online]. Available: https://doi.org/10.1080/00295450.2022.2043087.

[28] H. Trellue, C. Taylor, E. Luther, *et al.*, "Advancements in Yttrium Hydride Moderator Development," *Nuclear Technology*, vol. 209, no. sup1, S123–S135, 2023, ISSN: 19437471. DOI: 10.1080/00295450.2022.2043088.

[29] T. J. Morton, M. McKellar, P. Sabharwall, and S. Jaison, "Development, Construction, and Operation of the Agile Non-nuclear Microreactor Experimental Test Bed (MAGNET) and Helium Component Test Facility (He-CTF)," *Nuclear Science and Engineering*, vol. 00, no. 00, pp. 1–11, 2024, ISSN: 1943748X. DOI: 10.1080/00295639.2024.2384218.

[30] General Atomics, "Graphite design handbook," *DOE-HTGR-88111*, pp. 1–122, 1988, ISSN: 1091-4269.

[31] P. R. Geimer, A. A. Delorey, L. B. Beardslee, and T. J. Ulrich, "Demonstration of acoustic monitoring for structural health of microreactors: Through use of neural networks and resonant ultrasound spectroscopy," Los Alamos National Laboratory, Tech. Rep., 2023, LA–UR–23–26 860.

[32] E. B. Flynn, S. Y. Chong, G. J. Jarmer, and J. R. Lee, "Structural imaging through local wavenumber estimation of guided waves," *NDT and E International*, vol. 59, pp. 1–10, 2013, ISSN: 09638695. DOI: 10.1016/j.ndteint.2013.04.003. [Online]. Available: http://dx.doi.org/10.1016/j.ndteint.2013.04.003.

[33] L. Beardslee, P. Shokouhi, and T. Ulrich, "Optimal measurement point selection for resonant ultrasound spectroscopy of complex-shaped specimens using principal component analysis," *NDT & E International*, vol. 141, no. October 2023, p. 103 000, Jan. 2024, ISSN: 09638695. DOI: 10.1016/j.ndteint.2023.103000. [Online]. Available: https://doi.org/10.1016/j.ndteint.2023.103000%20https://linkinghub.elsevier.com/retrieve/pii/S0963869523002153.

[34] D. Di Maio, P. Castellini, M. Martarelli, *et al.*, *Continuous Scanning Laser Vibrometry: A raison d'être and applications to vibration measurements*, Jul. 2021. DOI: 10.1016/j.ymssp.2020.107573.

[35] L. B. Beardslee, R. Schoenemann, M. Root, *et al.*, "Embedded acoustic sensing and monitoring techniques for small modular reactors," Los Alamos National Laboratory, Los Alamos National Laboratory LA-UR-22-30061, Tech. Rep., 2022, LA–UR–22–30 061.

[36] J. Kossaifi, N. B. Kovachki, K. Azizzadenesheli, and A. Anandkumar, "Multi-grid tensorized fourier neural operator for high- resolution PDEs," *Transactions on Machine Learning Research*, 2024, ISSN: 2835-8856. [Online]. Available: https://openreview.net/forum?id=AWiDlO63bH.